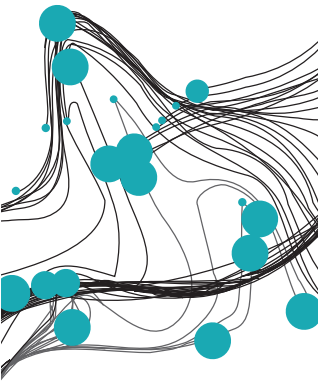

RAM ROBOTICS AND MECHATRONICS

Analysis of a 3D printed whisker-inspired tactile sensor

R.J. (Ralph) Brantjes

BSC ASSIGNMENT

Committee:
prof. dr. ir. G.J.M. Krijnen
G.J.W.Wolterink, MSc
dr. A.Sadeghi
dr. ir. B.J.F. Van Beijnum

July 2020

026RaM2020
Robotics and Mechatronics
EEMCS
University of Twente
P.O. Box 217
7500 AE Enschede
The Netherlands

UNIVERSITY OF TWENTE. | TECHMED CENTRE
UNIVERSITY OF TWENTE. | DIGITAL SOCIETY INSTITUTE

Abstract

Whiskers are very common features for animals; they are present in almost all mammals. There are various applications which would benefit from being able to mimic these whiskers. The specific application that will be discussed within this paper is the use of whiskers as a tactile force sensor. The system will be passive and will measure the force and distance at which a force is applied. The end goal of the sensor is to have the ability to measure 4 degrees of freedom. A more simple version of a tactile whisker sensor consisting of 2 DOF will be considered first. Within this report, the focus lies on creating a mechanical analysis of the system and simulating the behaviour of the whisker. The mechanical analysis of the whisker was then compared to the Ansys simulation of the whisker. The results of the comparison of the mechanical analysis and the simulation of the whisker lie close to each other, meaning that the whisker behaviour derived from the mechanical analysis in this report can be used in the future. Especially the 4 DOF mechanical model shows a lot of similarities with the simulations.

Preface

This report has been written in Juli 2020 in a 12 week bachelor thesis at the University of Twente under the supervision of Gijs Krijnen and Gerjan Wolterink.
During this thesis, a mechanical analysis and simulations were made for the design of a 3D-printed whisker-inspired tactile sensor.
I would like to thank Gijs Krijnen and Gerjan Wolterink very much for helping me throughout this thesis and for being part of my bachelor assignment committee. I would also like to thank the Robotics and Mechatronics group for providing me with useful information and help within my thesis. Lastly, I would like to thank Dr. A. Sadeghi and Dr. B.J.F. Van Beijnum for being part of my bachelor assignment committee.

Ralph Brantjes
University of Twente, 10/07/2020

Contents

1 Introduction

1.1 Context

Whiskers are very common features for animals; they are present in almost all mammals, sometimes even before birth. Whiskers can have different purposes depending on the animal. They can for example permit animals to sense the spacial coordinates of an object, their shape and their texture. A rat's whisker is able to detect small differences in surface textures at a comparable level to human fingertips. They achieve this by sweeping their whiskers in a rhythmic forward and backward motion called whisking. [1, 2] Seals are able to analyze water movements using their whiskers. This way they can sense movement of prey fish or they can follow the movement left behind by objects that have passed by earlier. [3]
There are various applications which would benefit from being able to mimic these whiskers but there is not yet a sensor good enough to precisely mimic the whisker behaviour. This is a problem because especially navigating areas filled with smoke or dust (which could hinder other sensors) could make very good use of whisker-inspired sensors as they can sense exactly where a wall is. Whiskers also have useful medical purposes. They can for example be used to enhance the precision of robotic heart surgery [4]. The specific application that will be discussed within this report is the use of whiskers as a tactile force sensor. The system will be passive and will measure the force and distance at which a force is applied.

The sensor will be 3D printed as this enables easy reproduction of a sensor in a very cost-effective way. Additionally, 3D printing makes it very easy to make changes in the design if necessary. 3D printing also enables the creation of certain complicated designs otherwise not possible to make. The downsides of 3D printing is the fact that it is quite a slow process and the end product can handle less stress compared to structures fabricated with the help of other techniques.
The final sensor will measure 4 degrees of freedom (henceforth referred to as DOF). These four degrees are the movement in the x-direction, the movement in the y-direction, the rotation around the x-axis and the rotation around the y-daxis. Before this is achieved, a 2 DOF sensor will be discussed as this is a much simpler sensor and will therefore provide an adequate build-up to the full 4 DOF sensor.

1.1.1 Previous research

Multiple research papers have already been published on the biomimicry of whiskers. Many of these papers make use of active whisker sensors. A few examples of the use of passive whiskers exist. There are not yet any papers on the creation of a whisker inspired 4 DOF tactile sensor using strain gauges that has been 3D-printed except for the bachelor assignment that has been done before this one [5] and a few others within the Robotics and Mechatronics group such as the one of B.Eijking [6] who made a 2 DOF version.
Harada et al. [7] have made a printed 2D whisker inspired sensor using temperature sensors and strain sensors that are able to distinguish the profile of a surface with an accuracy of around 59 % per Pascal. The design would unfortunately not work in the way that will be researched within this report because they used multiple flat whiskers in their design and incorporated the sensors into the whisker. This is not possible for a 4 DOF sensor as it needs to be able to be agitated in multiple directions.
Lungarella et al. [8] have created an artificial whisker based on changes in distance between capacitor plates attached to the base of the whisker. This study found that the use of different materials as whisker will result in a different complexity of the results mostly due to the stiffness

of the material. This could prove to have an impact on the end result. Another important factor is found to be the shape of the whisker. A straight-lined whisker is is found to be more capable of distinguishing a surface compared to a curved one. Therefore, the choice is made to keep the whisker straight for this design. [9] The straight line whisker also makes more sense to use for a 4 DOF sensor as it can be symmetrical in the xy-plane.

1.2 Goals and Approach

1.2.1 Goals

The overall goal of this bachelor assignment is to evaluate how 3D-printing can be used to make whisker inspired tactile sensors. For this, the different aspects of the production have to be considered. This assignment will elaborate on previous work done by J. Tichelaar [5]. He made designs for a 2 DOF and 4 DOF sensor but the mechanical analysis is still lacking and thus, the focus will primarily lie on a more in depth analysis of the mechanical behaviour of a 2 DOF and 4 DOF tactile sensor. The main research question to be answered within this report is as follows: 'What are the relations between applied forces and moments on the deformations of a whisker-inspired structure?'
This question can be dissected into multiple smaller research questions:

- Up until what loading of the whisker beam will the relations be linear?
- To what degree are the relations between applied forces and moments on the deformations of a whisker-inspired structure invertable?
- What are the differences between the mechanical model and the simulations of a 3D-printed tactile whisker sensor in 2 DOF and 4 DOF?

In order to answer the questions above, there are a few steps to go through. These steps have been listed below.

- Make a mechanical analysis of a 2 DOF and a 4 DOF sensor.
- Create an adequate simulation model of a 2 DOF and a 4 DOF sensor.
- Compare the simulations with the mechanical model for both the 2 DOF and 4 DOF sensors.

1.3 Outline

This report will first introduce a design of the tactile sensor. It will then elaborate the design by presenting an Ansys simulation model and a comparable mechanical model. Then the fabrication process will be elaborated on. As the whisker has not been physically created[1], the section will give a theoretical input on the fabrication of both the 2 DOF and 4 DOF tactile sensor. The report will then go on to the final results. Here, the mechanical model will be compared to the simulation model. The final part of this report is the discussion and the conclusion.

[1] This BSc project was carried out in the spring of 2020 when the university's lab-facilities were closed due to the Covid-19 crisis.

2 Design

Within this chapter, the design choices of the whisker will be discussed. The full whisker design can be divided into two parts. The first part being the whisker itself and the second part the base of the whisker. First of all, the whisker itself will be discussed. Then, this section of the report will discuss the designs of the 2 DOF and the 4 DOF whisker base into detail.

2.1 Whisker design

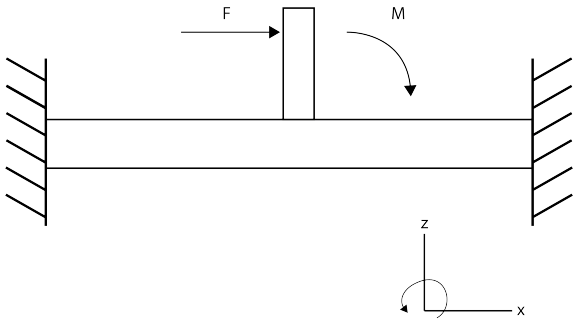

Figure 2.1: Schematic representation of the 2DOF whisker with a force applied.

The whisker itself is designed as a simple vertical beam. A representation of the full 2 DOF whisker is given in figure 2.1. The whisker functions as a tool to bend the beam at the base when a force is applied to it. At some height on this whisker, a force is applied; this force will transfer into a moment and a force on the base of the whisker, bending the base. The whisker is designed as a cuboid beam in the 2 DOF case. The whisker can only be pushed in two directions making a cuboid shape ideal. For the 4 DOF whisker beam, the whisker will be cylindrical. This is simply because a cylindrical shape will warp less. More information on warping is given in the fabrication section 5.2 of this paper.

2.2 2 DOF whisker

The 2 DOF beam looks like a simple cuboid beam with the whisker in the middle. A representation of the beam can be seen in figure 2.1. The length of the beam at the base for both the 2 DOF and 4 DOF has been taken as 50 mm and the thickness as 2 mm. An important aspect to keep in mind for the beam is to carefully consider the ratio between the length and the thickness of the beam because a longer beam will respond more like an Euler-Bernouilli beam. This is beneficial because Euler-Bernouilli is a linear slender beam approximation. The beam will therefore be simpler to analyze and more linear. A longer beam will bend more and show a bigger displacement in the x-direction. This will make your sensors pick up a better signal thus improving the accuracy of the measurements. The downside to a long beam is that the construction will become less sturdy. If the beam is too weak, it will likely sag or make unpredictable movements. Additionally, the longer the beam, the bigger the base of the whisker will be. This means it is harder to use it in some applications due to its bulkiness.
When the length to thickness ratio is too small, non-linear effects will occur and the beam will veer away from from the Euler-Bernoulli beam approximation and require the more involved non-linear Timoshenko beam approximation. To make an estimation of the results, a comparison has been made between the two by looking at the maximum tip deflection of both. [10]
For the maximum tip deflection of an Euler-Bernouilli beam:

$$U^B(L) = \frac{4FL^3}{Et^3} \tag{2.1}$$

And for the maximum tip deflection of a Timoshenko beam:

$$U^T(L) = \frac{4FL^3}{Et^3} + \frac{12FL}{5Et} \tag{2.2}$$

With $U(x)$ the deflection in the z-direction, E the Young's modulus, L the length of the beam and t the thickness of the beam. Due to the extra term on the Timoshenko beam is due to the extra shear deformation within the beam. The ratio will then be:

$$f = \frac{U^T(L)}{U^B(L)} = 1 + \frac{3}{5}\left(\frac{t}{L}\right)^2 \tag{2.3}$$

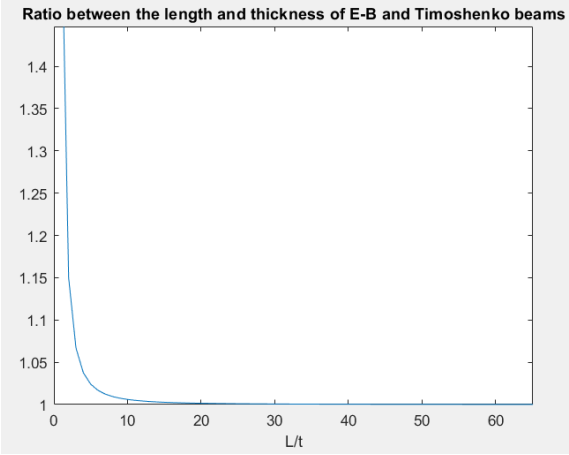

Figure 2.2: The rate at which the maximum deflection at the tip of a beam Timoshenko and Euler-Bernouilli differ based on the length over the thickness of a beam. At a ratio L/t of about 18, the Euler-Bernouilli and Timoshenko beams will behave the same. [10]

The case that is illustrated in this report consists of a fixed-fixed beam. Unfortunately, the ratio between Euler-Bernouilli and Timoshenko beams has not been found for fixed-fixed beams. Therefore, an educated guess was made. When comparing the two cases, the maximum deflection of a fixed-fixed beam is smaller at similar load than for the fixed-free beam.
Maximum deflection of a fixed-fixed beam:

$$\delta_{max} = \frac{Pl^3}{48EI} \tag{2.4}$$

Maximum deflection of a fixed-free beam:

$$\delta_{max} = \frac{Pl^3}{3EI} \tag{2.5}$$

From equations 2.4 and 2.5 can be seen that at a similar load, the maximum deflection of a fixed-fixed beam is 16 times smaller. The beam will therefore bend less and have a smaller maximum deflection.
From figure 2.3 can be seen that the difference between Euler-Bernouilli beams and Timoshenko beams will increase as the deflection of the beam increases. A smaller deflection will mean a smaller difference between Euler-Bernouilli beams and Timoshenko beams.
Figure 2.2 illustrates that, from a length over thickness ratio of about 18 and bigger, there will be practically no difference between Euler-Bernouilli beams and Timoshenko beams. The ratio used in this paper is 25. Having just derived that the difference between Euler-Bernouilli beams and Timoshenko beams will be even smaller for a fixed-fixed beam, only the Euler-Bernouilli beam equation is used in this paper.

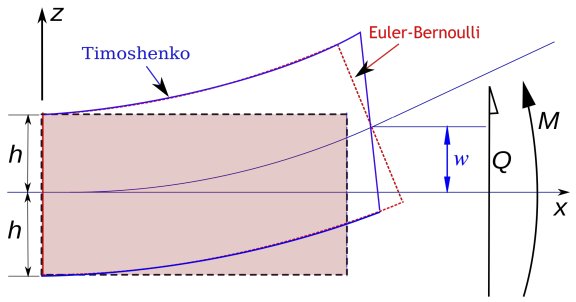

Figure 2.3: Comparison between a Timoshenko and an Euler-Bernouilli beam analysis. [11]

2.3 4 DOF whisker

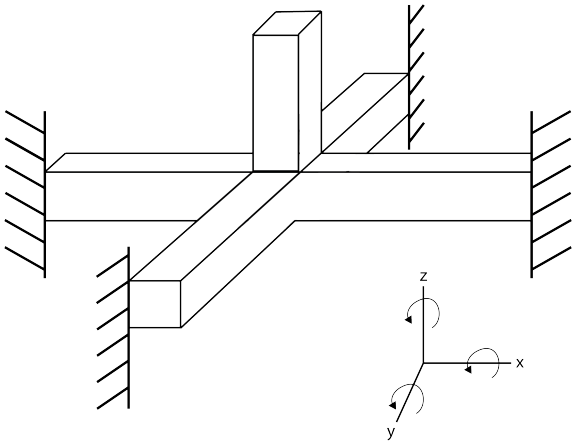

Figure 2.4: Schematic representation of the 4DOF whisker base.

The 4 DOF whisker structure looks like a cross beam with the whisker sticking out from the middle of the cross. A representation of this can be found in figure 2.4. Note that during this paper, the definitions of the axis will be such as depicted in figure 2.4. This beam has the same dimensions as the 2 DOF whisker with a beam thickness of 2 mm and a total length of 50 mm. The different structure will make a difference in the equations of the 2 DOF beam due to the additional beam crossing the middle of the whisker base. It is therefore expected that the angle at the middle of the beam will be smaller than the 2 DOF beam due to the extra torsion introduced by the side beams. The deflection will also be smaller due to the extra force needed to push the side beams.
In order to create a simpler model of the mechanical beam analysis, the whisker itself has been omitted and the structure is modeled as a plain cross beam.

3 Theory

This chapter will introduce the beam theory used in this report. It will first go through the derivation of the 2 DOF mechanical model of the force in the z-direction and the moment around the y-axis for the whisker. This model will then be elaborated on by adding the deflection due to a force in the x-direction. From the basis of the 2 DOF model, the 4 DOF model is derived. This adds torsion to the beam and combines multiple aspects of the 2 DOF derivation together.
The main theory used to derive an expression for the beams is the Galerkin finite element method.

3.1 Full derivation of the beam element equation for the 2 DOF beam

In order to derive an expression for the beam, firstly, a global expression is considered for a piece of a rectangular beam.

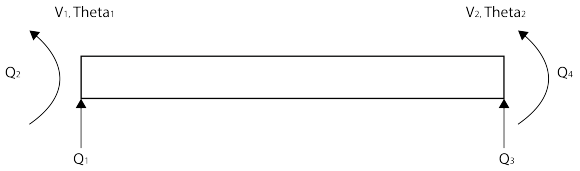

Figure 3.1: Schematic representation of an arbitrary piece of rectangular beam.

At each of the sides of the beam, there is a deflection v and an angle θ. The corresponding forces and moments on the sides are Q_1, Q_3 and Q_2, Q_4 respectively. The reason these are all depicted as Q is seen further on in the equation.
Using the Galerkin method for beams, the equation can be simplified. The method for an Euler-Bernouilli beam is fully worked out below. This method can also be used with Timoshenko beams but it is more complicated to work out.

The equation 4.1 will be called $R(x)$. $R(x)$ can be applied to a certain part of a beam. The length of this part will be called L. Keep in mind that L is the length of the beam part that is being analysed and not the full length of the total beam. By applying the Galerkin method of integration, the equation will look as follows: [12]

$$\int_0^L R(x)\,v(x)\,dx = \int_0^L \left\{ \frac{d^2}{dx^2}\left(EI\frac{d^2w}{dx^2} \right) - q \right\} v(x)\,dx \tag{3.1}$$

This is called the strong form Galerkin. Where $v(x)$ is a weight function that changes over the length over the beam and q is a load. This weight function is evaluated over the whole part of the beam. The specific application for this weight function is explained below.
In order to continue, a formulation for the weak form Galerkin has to be formed. This will reduce the highest order from fourth to two second order equations. This is done by integrating by parts twice:

$$G[w(x), v(x)] = \int_0^L \left\{ \left(EIw''(x) \right)'' - q \right\} v(x)\,dx = 0 \tag{3.2}$$

Is rewritten and simplified as the equation below by integration by parts:

$$G[w(x), v(x)] = \int_0^L \left\{ \left(EIw''(x) \right) v''(x) - qv(x) \right\} dx + \left[v(x) \left(EIw''(x) \right)' \right]_0^L - \left[v'(x) \left(EIw''(x) \right) \right]_0^L = 0 \tag{3.3}$$

And finally to:

$$G[w(x),v(x)] = \int_0^L \left\{\left(EIw''(x)\right)v''(x) - qv(x)\right\}dx + v(L)V(L) - v(0)V(0) - v'(L)M(L) + v'(0)M(0) = 0 \tag{3.4}$$

Where the essential boundary conditions ($v(x)$ and $v'(x)$) can be observed. The natural BC can also be observed with the moment M being $EIw''(x)$ and the shear V being $(EIw''(x))'$.
Now that the weak form is obtained, the directions of the shear and moment are changed to match the positive direction of the defined axis as seen in figure 3.1 to make the calculations easier. [13] This is why the definitions below are taken:

$$Q_1 = V(0) = (EIw''(0))' \tag{3.5}$$

$$Q_2 = -M(0) = -EIw''(0) \tag{3.6}$$

$$Q_3 = -V(L) = -(EIw''(L))' \tag{3.7}$$

$$Q_4 = M(L) = EIw''(L) \tag{3.8}$$

Making the final weak form:

$$G[w(x),v(x)] = \int_0^L \left\{\left(EIw''(x)\right)v''(x) - qv(x)\right\}dx - v(L)Q_3 - v(0)Q_1 - v'(L)Q_4 - v'(0)Q_2 = 0 \tag{3.9}$$

4 nodal quantities can be distinguished that have to be continuous across the element boundaries. These are $v(L), v(0), v'(L), v'(0)$. In order to find out the values of these quantities, an approximation function is created. There are 4 unknown quantities. That is why a trial function through these quantities can be a cubic polynomial.

$$w(x) = c_0 + c_1(x/L) + c_2(x/L)^2 + c_3(x/L)^3 \tag{3.10}$$

Then the boundary conditions are imposed on the function.

$$w(0) = c_0 = v_1 \tag{3.11}$$

$$w'(0) = c_1(1/L) = \theta_1 \tag{3.12}$$

$$w(L) = c_0 + c_1 + c_2 + c_3 = v_2 \tag{3.13}$$

$$w'(L) = c_1/L + 2c_2/L + 3c_3/L = \theta_2 \tag{3.14}$$

Writing this in matrix form and then inverting the matrix gives:

$$\begin{bmatrix} c_0 \\ c_1 \\ c_2 \\ c_3 \end{bmatrix} = \begin{pmatrix} 1 & 0 & 0 & 0 \\ 0 & 1/L & 0 & 0 \\ 1 & 1 & 1 & 1 \\ 0 & 1/L & 2/L & 3/L \end{pmatrix}^{-1} \begin{bmatrix} v_1 \\ \theta_1 \\ v_2 \\ \theta_2 \end{bmatrix}$$

Equals to:

$$\begin{bmatrix} c_0 \\ c_1 \\ c_2 \\ c_3 \end{bmatrix} = \begin{pmatrix} 1 & 0 & 0 & 0 \\ 0 & L & 0 & 0 \\ -3 & -2L & 3 & -L \\ 2 & L & -2 & L \end{pmatrix} \begin{bmatrix} v_1 \\ \theta_1 \\ v_2 \\ \theta_2 \end{bmatrix}$$

$w(x)$ can now be expressed in v and θ in the form of:

$$w(x) = v_1 N_1 + \theta_1 N_2 + v_2 N_3 + \theta_2 N_4 \tag{3.15}$$

And so in matrix form:

$$w(x) = \begin{bmatrix} N_1 & N_2 & N_3 & N_4 \end{bmatrix} \begin{bmatrix} v_1 \\ \theta_1 \\ v_2 \\ \theta_2 \end{bmatrix} = \mathbf{Nd}$$

Where the N_i's are basis functions. These functions are used to express the polynomial into v and θ. These can be derived in the following way: [14]

$$N_1 = \frac{dw}{dv_1}, N_2 = \frac{dw}{d\theta_1}, N_3 = \frac{dw}{dv_2}, N_4 = \frac{dw}{d\theta_2} \tag{3.16}$$

This results in the following basis functions:

$$N_1(x) = 1 - \frac{3x^2}{L^2} + \frac{2x^3}{L^3}, N_2(x) = x - \frac{2x^2}{L} + \frac{x^3}{L^2}, N_3(x) = \frac{3x^2}{L^2} - \frac{2x^3}{L^3}, N_4 = -\frac{x^2}{L} + \frac{x^3}{L^2} \tag{3.17}$$

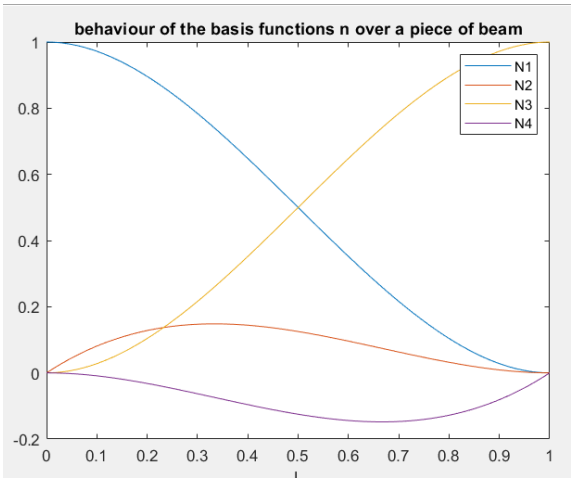

Figure 3.2: Representation of the magnitude of $N1$, $N2$, $N3$ and $N4$ over a piece of beam.

For the weak Galerkin form equation, the second order derivative of the deflection is needed. For convenience, the second derivative of the basis functions are called **B**.

$$w(x)'' = \begin{bmatrix} N_1'' & N_2'' & N_3'' & N_4'' \end{bmatrix} \begin{bmatrix} v_1 \\ \theta_1 \\ v_2 \\ \theta_2 \end{bmatrix} = \mathbf{Bd}$$

Plugging the result back into the weak Galerkin form results in one equation for every N. There are thus 4 equations and 4 unknowns.

$$\int_0^L \left\{EI\mathbf{B}\mathbf{d}N_1''(x) - qN_1\right\} dx - N_1(L)Q_3 - N_1(0)Q_1 - N_1'(L)Q_4 - N_1'(0)Q_2 = 0$$

$$\int_0^L \left\{EI\mathbf{B}\mathbf{d}N_2''(x) - qN_2\right\} dx - N_2(L)Q_3 - N_2(0)Q_1 - N_2'(L)Q_4 - N_2'(0)Q_2 = 0$$

$$\int_0^L \left\{EI\mathbf{B}\mathbf{d}N_3''(x) - qN_3\right\} dx - N_3(L)Q_3 - N_3(0)Q_1 - N_3'(L)Q_4 - N_3'(0)Q_2 = 0$$

$$\int_0^L \left\{EI\mathbf{B}\mathbf{d}N_4''(x) - qN_4\right\} dx - N_4(L)Q_3 - N_4(0)Q_1 - N_4'(L)Q_4 - N_4'(0)Q_2 = 0$$

Using the equation 3.1, and the fact that only one of the N terms in front of the loads is 1 at one time, the equation can be simplified to:

$$\int_0^L \left\{EI\mathbf{B}^T\mathbf{B}\mathbf{d} - q\mathbf{N}^T\right\} dx - \mathbf{Q} = 0 \tag{3.18}$$

where

$$\mathbf{Q} = \begin{bmatrix} Q_1 & Q_2 & Q_3 & Q_4 \end{bmatrix}^T$$

The final equation results in:

$$\int_0^L EI\mathbf{B}^T\mathbf{B}dx\mathbf{d} = \int_0^L (q\mathbf{N}^T)dx + \mathbf{Q} \tag{3.19}$$

Working out the first integral and writing this in matrix form will result in the following general equation for a piece of rectangular beam [15]:

$$\frac{2EI}{L^3}\begin{pmatrix} 6 & -3L & -6 & -3L \\ -3L & 2L^2 & 3L & L^2 \\ -6 & 3L & 6 & 3L \\ -3L & L^2 & 3L & 2L^2 \end{pmatrix}\begin{bmatrix} v_1 \\ \theta_1 \\ v_2 \\ \theta_2 \end{bmatrix} = \int_0^L q \begin{bmatrix} 1 - \frac{3x^2}{L^2} + \frac{2x^3}{L^3} \\ x - \frac{2x^2}{L} + \frac{x^3}{L^2} \\ \frac{3x^2}{L^2} - \frac{2x^3}{L^3} \\ -\frac{x^2}{L} + \frac{x^3}{L^2} \end{bmatrix} dx + \begin{bmatrix} Q_1 \\ Q_2 \\ Q_3 \\ Q_4 \end{bmatrix} \tag{3.20}$$

This beam formulation can be used for any part of a beam. With this formulation, the angle and the deflection can be related to the forces and the moments on the beam. The formulation will now be used on the beam as used for the 2 DOF whisker seen in figure 3.3. As there is no distributed load over the beam, part of equation 3.20 is 0.

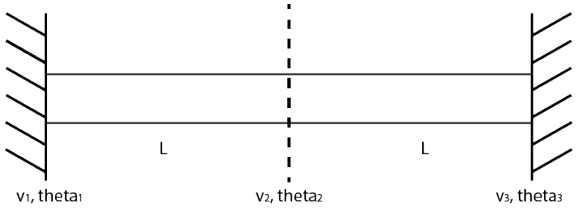

Figure 3.3: Splitting the 2 DOF beam into two beam elements of equal length.

$$\begin{bmatrix} P_1 \\ M_1 \\ P_2 \\ M_2 \\ P_3 \\ M_3 \end{bmatrix} = \frac{2EI}{L^3} \begin{pmatrix} 6 & -3L & -6 & -3L & 0 & 0 \\ -3L & 2L^2 & 3L & L^2 & 0 & 0 \\ -6 & 3L & 6+6 & 3L-3L & -6 & -3L \\ -3L & L^2 & 3L-3L & 2L^2+2L^2 & 3L & L^2 \\ 0 & 0 & -6 & 3L & 6 & 3L \\ 0 & 0 & -3L & L^2 & 3L & 2L^2 \end{pmatrix} \begin{bmatrix} v_1 \\ \theta_1 \\ v_2 \\ \theta_2 \\ v_3 \\ \theta_3 \end{bmatrix} \tag{3.21}$$

Then by applying the BC of

$$v_1 = 0, \theta_1 = 0, v_3 = 0, \theta_3 = 0$$

there is only a simple equation left:

$$\begin{bmatrix} P_2 \\ M_2 \end{bmatrix} = \frac{2EI}{L^3} \begin{pmatrix} 12 & 0 \\ 0 & 4L^2 \end{pmatrix} \begin{bmatrix} v_2 \\ \theta_2 \end{bmatrix} \tag{3.22}$$

This is the equation that relates the angle to the moment at the middle of the beam. It can be observed that the angle of the system is linear to the moment. This is only correct when considering very small moments due to the forces that occur when the displacement of the beam is restricted.

The whisker is not only subject to a moment around the y-axis, but also to a force in the x direction. To model this, the same Galerkin approach is taken.
By using the equation for the stretching and compression of rods.

$$(EAu')' + p = 0 \tag{3.23}$$

Where E is young's modulus, A the cross-sectional area in m^2 and u the deflection in the x-direction and p the force in the x-direction in N.
Deriving the weak form Galerkin by integration by parts of the strong form gives:

$$\int_0^L (-EAu'v' + pv)dx + [vEAu']_0^L = \int_0^L (-EAu'v' + pv)dx - v(L)P_L - v(0)P_0 = 0 \tag{3.24}$$

$$P_L = EAu(L)', -P_0 = EAu(0)'$$

In this case, there are only 2 essential BC's ($v(0), v(L)$) and 2 natural BC's (EAu' at L and at 0). This all means that the approximation function u taken can be linear.

$$u(x) = c_0 + c_1 x \tag{3.25}$$

$$u(x_1) = c_0 + c_1 x_1 = u_1 \tag{3.26}$$

$$u(x_2) = c_0 + c_1 x_2 = u_2 \tag{3.27}$$

The unknown coefficients then are written in the form of u and x.

$$x_1 - x_2 = -L \tag{3.28}$$

$$c_1 = \frac{u_1 - u_2}{x_1 - x_2} \tag{3.29}$$

$$c_0 = u_2 - \frac{u_1 - u_2}{x_1 - x_2} x_2 \tag{3.30}$$

Resulting in the approximation function:

$$u(x) = u_2 + \frac{u_1 - u_2}{L}x_2 - \frac{u_1 - u_2}{L}x = u_1\frac{u_2 - x}{L} + u_2\frac{x - x_1}{L} \tag{3.31}$$

What can be seen is that the approximation above satisfies the essential BC's.

$$u(x) = u_1\frac{u_2 - x}{L} + u_2\frac{x - x_1}{L} = u_1N_1(x) + u_2N_2(x) = v(x) = \begin{bmatrix} N_1 & N_2 \end{bmatrix}\begin{bmatrix} u_1 \\ u_2 \end{bmatrix} = \mathbf{Nd} \tag{3.32}$$

It can be seen that $N(x)$ satisfies kronecker delta properties and only one component will be 1 at each of the edges of the beam.

$$\frac{\partial u(x)}{\partial x} = \mathbf{Bd}$$

Substituting this back into the weak galerkin form gives:

$$G[u(x), N(x)] = \int_{x_1}^{x_2}(EA\mathbf{Bd}\frac{\partial N_i(x)}{\partial x} - pN_i(x))dx - P_i \tag{3.33}$$

With i = 1,2. There are 2 equations and 2 unknowns therefore it is solvable. Putting the final result in matrix form results in:

$$G[u(x), N(x)] = \int_{x_1}^{x_2}(EA\mathbf{B}^T\mathbf{B})dx = \int_{x_1}^{x_2} p\mathbf{N}^T dx + \mathbf{P} \tag{3.34}$$

$$\mathbf{P} = \begin{bmatrix} P_1 \\ P_2 \end{bmatrix}$$

$$\mathbf{B} = \begin{bmatrix} \frac{\partial N_1(x)}{\partial x} & \frac{\partial N_2(x)}{\partial x} \end{bmatrix} = \begin{bmatrix} \frac{-1}{L} & \frac{1}{L} \end{bmatrix}$$

$$\frac{EA}{L}\begin{pmatrix} 1 & -1 \\ -1 & 1 \end{pmatrix}\begin{bmatrix} u_1 \\ u_2 \end{bmatrix} = \int_{x_1}^{x_2} p\begin{bmatrix} N_1 \\ N_2 \end{bmatrix} + \begin{bmatrix} P_1 \\ P_2 \end{bmatrix} \tag{3.35}$$

Using this form, it is possible to evaluate the deflection in the x-direction of the whisker. The matrix is obtained using the same diagram as for the moment.

$$\begin{bmatrix} P_1 \\ P_2 \\ P_3 \end{bmatrix} = \frac{EA}{L}\begin{pmatrix} 1 & -1 & 0 \\ -1 & 1+1 & -1 \\ 0 & -1 & 1 \end{pmatrix}\begin{bmatrix} u_1 \\ u_2 \\ u_3 \end{bmatrix} \tag{3.36}$$

Then applying the BC's of $u_1 = 0, u_3 = 0$ results in:

$$F = \frac{2EA}{L}u_2 \tag{3.37}$$

This is consistent with literature [16].

3.2 Derivation of the 4 DOF beam element equations.

The standard formula for the torsion of a beam can be used to evaluate how the total cross beam will behave.

$$T = \frac{GJ}{L}\phi$$

[17] Where T is the torsion in Nm, J is the second moment of area in m^4, L the length in m, G the shear modulus in Pascal and ϕ the angle of twist in radians. First, a simple beam is considered where a torsion is applied to both ends 3.4.

This is then simplified into two situations. A beam clamped at the left side with a torsion on the right side 3.5 and a beam clamped on the right side with a torsion on the left side 3.6.

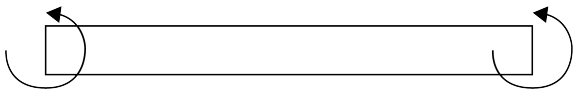

Figure 3.4: Beam element with a torsion applied at both sides

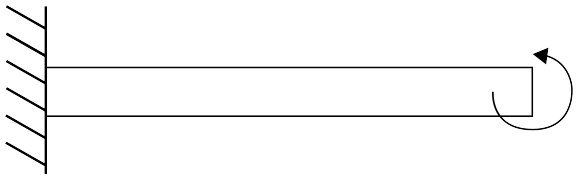

Figure 3.5: Beam element with a torsion applied at both sides

For the first beam we apply one BC, namely $\phi_1 = 0$. The relation will then be as follows [17]:

$$M_{T2} = \frac{GJ}{L}\phi_2 \tag{3.38}$$

$$M_{T1} = -M_{T2} = -\frac{GJ}{L}\phi_2 \tag{3.39}$$

Then for the second part, the BC is that $\phi_2 = 0$. This will result in:

$$M_{T1} = \frac{GJ}{L}\phi_1 \tag{3.40}$$

$$M_{T2} = -M_{T1} = -\frac{GJ}{L}\phi_1 \tag{3.41}$$

To get the final relation for the beam with torsion on both ends, the two parts are simply superimposed. This results in the final relation.

$$\begin{bmatrix} M_{T1} \\ M_{T2} \end{bmatrix} = \begin{pmatrix} \frac{GJ}{L} & -\frac{GJ}{L} \\ -\frac{GJ}{L} & \frac{GJ}{L} \end{pmatrix} \begin{bmatrix} \phi_1 \\ \phi_2 \end{bmatrix} \tag{3.42}$$

Now that this relation has been established. The standard stiffness matrix for an arbitrary piece of rectangular beam can be elaborated on. [17]

$$\begin{bmatrix} Q_1 \\ Q_2 \\ Q_3 \\ Q_4 \\ Q_5 \\ Q_6 \end{bmatrix} = \begin{pmatrix} \frac{12EI}{L^3} & -\frac{6EI}{L^2} & 0 & -\frac{12EI}{L^3} & -\frac{6EI}{L^2} & 0 \\ -\frac{6EI}{L^2} & \frac{4EI}{L} & 0 & \frac{6EI}{L^2} & \frac{2EI}{L} & 0 \\ 0 & 0 & \frac{GJ}{L} & 0 & 0 & -\frac{GJ}{L} \\ -\frac{12EI}{L^3} & \frac{6EI}{L^2} & 0 & \frac{12EI}{L^3} & \frac{6EI}{L^2} & 0 \\ -\frac{6EI}{L^2} & \frac{2EI}{L} & 0 & \frac{6EI}{L^2} & \frac{4EI}{L} & 0 \\ 0 & 0 & -\frac{GJ}{L} & 0 & 0 & \frac{GJ}{L} \end{pmatrix} \begin{bmatrix} v_1 \\ \theta_1 \\ \phi_1 \\ v_2 \\ \theta_2 \\ \phi_2 \end{bmatrix} \tag{3.43}$$

Last of all, the equation for deflection due to a force in the x-direction (equation 4.3) can also be added into this matrix:

$$\begin{bmatrix} Q_1 \\ Q_2 \\ Q_3 \\ Q_4 \\ Q_5 \\ Q_6 \\ Q_7 \\ Q_8 \end{bmatrix} = \begin{pmatrix} \frac{EA}{L} & 0 & 0 & 0 & -\frac{EA}{L} & 0 & 0 & 0 \\ 0 & \frac{12EI}{L^3} & -\frac{6EI}{L^2} & 0 & 0 & -\frac{12EI}{L^3} & -\frac{6EI}{L^2} & 0 \\ 0 & -\frac{6EI}{L^2} & \frac{4EI}{L} & 0 & 0 & \frac{6EI}{L^2} & \frac{2EI}{L} & 0 \\ 0 & 0 & 0 & \frac{GJ}{L} & 0 & 0 & 0 & -\frac{GJ}{L} \\ -\frac{EA}{L} & 0 & 0 & 0 & \frac{EA}{L} & 0 & 0 & 0 \\ 0 & -\frac{12EI}{L^3} & \frac{6EI}{L^2} & 0 & 0 & \frac{12EI}{L^3} & \frac{6EI}{L^2} & 0 \\ 0 & -\frac{6EI}{L^2} & \frac{2EI}{L} & 0 & 0 & \frac{6EI}{L^2} & \frac{4EI}{L} & 0 \\ 0 & 0 & 0 & -\frac{GJ}{L} & 0 & 0 & 0 & \frac{GJ}{L} \end{pmatrix} \begin{bmatrix} u_1 \\ v_1 \\ \theta_1 \\ \phi_1 \\ u_2 \\ v_2 \\ \theta_2 \\ \phi_2 \end{bmatrix} \tag{3.44}$$

Figure 3.6: Beam element with a torsion applied at both sides

This identity matrix is however in local coordinates. In order to properly model the 4DOF, these equations have to be written in global coordinates (see AppendixB), namely $u,v,w,\phi_x,\phi_y,\phi_z$. By shifting the coordinates in a way that the 4 beam parts that can be seen in figure 3.7 can be evaluated. This is done by looking at the 4 DOF beam as two 2 DOF beams that intertwine in the middle. These beam elements can be combined in the same way as can be seen for the 2 DOF case. Doing this results in the matrix 7.1 below.

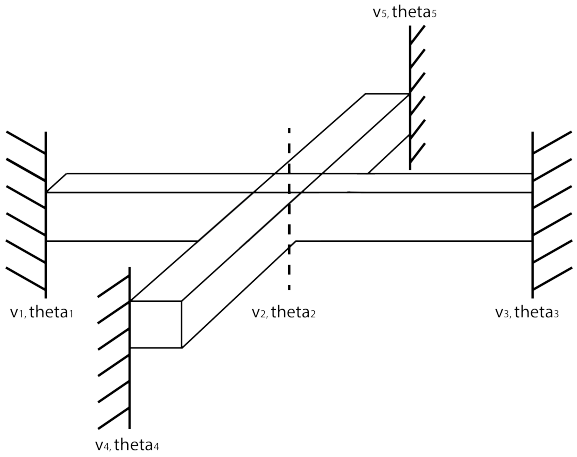

Figure 3.7: The 4 DOF beam split into 4 different elements.

$$\begin{bmatrix} F_x \\ F_y \\ F_z \\ M_x \\ M_y \\ M_z \end{bmatrix} = \begin{pmatrix} \frac{24EI}{L^3} + \frac{2EA}{L} & 0 & 0 & 0 & 0 & 0 \\ 0 & \frac{24EI}{L^3} + \frac{2EA}{L} & 0 & 0 & 0 & 0 \\ 0 & 0 & \frac{48EI}{L^3} & 0 & 0 & 0 \\ 0 & 0 & 0 & \frac{8EI}{L} + \frac{2GJ}{L} & 0 & 0 \\ 0 & 0 & 0 & 0 & \frac{8EI}{L} + \frac{2GJ}{L} & 0 \\ 0 & 0 & 0 & 0 & 0 & \frac{16EI}{L} \end{pmatrix} \begin{bmatrix} u \\ v \\ w \\ \phi_x \\ \phi_y \\ \phi_z \end{bmatrix} \tag{3.45}$$

From this, the impact of each of the forces and moments in all 6 DOF can be seen. These are the linear relations between the forces and moments applied on the structure. These relations can all be inverted in order to retrieve the force and moment from the angle and the deflection.

4 Model

This section is important for the report because it explains how the mechanical model has been obtained and the parameters used for the simulations. It will cover which simulation program was used and it will show the final mechanical model.
Both the simulation model and the analytical mechanical model follow the same principle. Because the model of the whisker is a static model, the force balance will equate to zero and no losses are present. Using this property, the initial force on the whisker can be split into two parts; the force acting in the x-direction of the whisker and the moment around the y-axis.
The force in the x-direction will result in a deflection of the beam. This deflection is modeled in the simulations and compared to the mechanical model for which an expression has been created for the same deflection. The moment around the y-axis will result in a beam deflection in the z direction. From the deflection around the middle of the beam, the angle is computed. A visual representation of this is given in figure 4.1. This angle is then compared with the expression derived in the mechanical model.

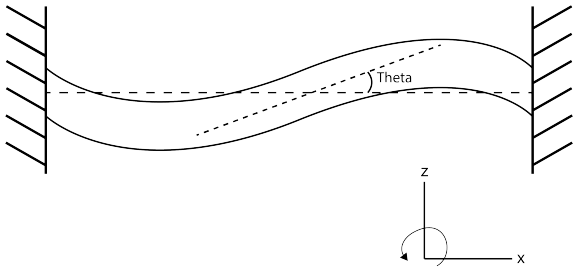

Figure 4.1: Representation of the beam under a moment. From the deflection profile, the angle theta in the middle can be computed.

4.1 Simulation model

Ansys was used for all the simulations of this report. The initial program to be used was Comsol. The program is comparable to Ansys and is perfectly capable of simulating simple beams. Unfortunately, due to Comsol not being available for students, the choice was made to look for another program to model the whisker. Another option as simulation program is Solidworks. The choice was made to use Ansys because it is much more geared towards finite element analysis than Solidworks.

4.1.1 2 DOF

The 2 DOF beam is modelled as a simple rectangular rod. The Ansys representation of the beam can be seen in figure 4.2. The mesh is taken to be 1 mm cuboids. This is done due to the simple nature of the beam. As stated above, the beam will be exposed to a force in the x-direction and a moment around the y-axis. An Ansys representation of the deflection caused by this force and this moment can be found in Appendix A. The two simulations are used in the result section in the report where the deflection in the x-direction and the y-angle are compared to the mechanical analysis.

4.1.2 4 DOF

The model of the 4 DOF simulation of the whisker base has been modeled in Ansys as a cross beam with a length of 50 mm and a thickness and hight of 2 mm. These are the same dimen-

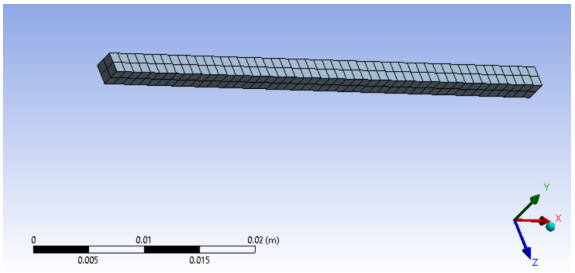

Figure 4.2: Ansys simulation model of the 2 DOF beam.

sions as the 2 DOF simulation beam. The Ansys model corresponding to the 4 DOF whisker cross beam is shown in figure 4.3. The beam was then subjected to a force in the x-direction and in a second simulation, the same beam is subjected to a moment around the y-axis. An Ansys representation of the deflection caused by this force and this moment can also be found in Appendix A. Similarly to the 2 DOF simulation, the results of the deflection in the x-direction and the y-angle are compared to the results of the mechanical analysis in order to validate the mechanical model.

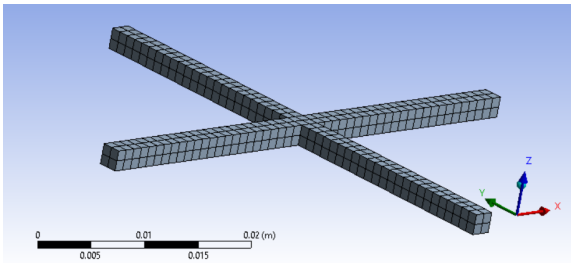

Figure 4.3: Ansys simulation model of the 4 DOF beam.

4.2 Mechanical model

4.2.1 2 DOF

Firstly, the deflection of the beam will be derived. The standard equation for the deflection of a beam is as follows [18]:

$$\frac{d^2}{dx^2}\left(EI\frac{d^2w}{dx^2}\right) - q = 0 \tag{4.1}$$

With q being the load in Newton, E being Young's modulus in Pascal, I the moment of inertia in mm^4 and w the deflection in meters. For the whisker, it can be said that the Young's modulus and the moment of inertia are constant throughout the beam.

The mechanical model for the 2 DOF has been derived in the theory section 3.1.

The final two equations to calculate the moment from the angle and the force in the x-direction from the displacement of the 2 DOF beam are:

$$\begin{bmatrix} P_2 \\ M_2 \end{bmatrix} = \frac{2EI}{L^3}\begin{pmatrix} 12 & 0 \\ 0 & 4L^2 \end{pmatrix}\begin{bmatrix} v_2 \\ \theta_2 \end{bmatrix} \tag{4.2}$$

$$F = \frac{2EA}{L}u_2 \tag{4.3}$$

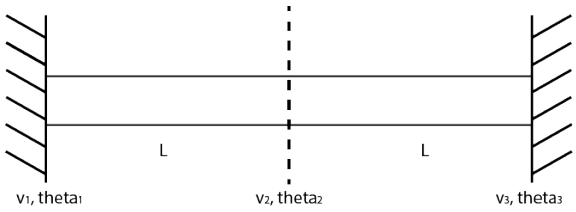

Figure 4.4: Splitting the 2 DOF beam into two elements of equal length

Where L is the length of one beam element (and not the full beam), A the area of the cross section of the beam, u the deflection of the beam in the horizontal direction and v the deflection of the beam in the vertical direction.
These equations are both linear and the square matrix make the equations invertible. This means that the force and the moment could be calculated from the displacement and the angle. The relations will be compared to the simulation data in order to validate the equations.

4.2.2 4 DOF

For the 4DOF situation, a beam is added on each side perpendicularly to the 2DOF beam. When the same moment is applied to the 4DOF cross beam, the beam will not only deflect, but also twist. This torsion moment that is applied is equal to the moment applied to the beam.

The full derivation of the 4 DOF beam equations can be found in the theory section 3.2.

This derivation ends up with the following element equation for the middle of the beam shown in figure 3.7. The element matrix is assuming that all the forces and moments present in the beam only originate from the middle. Effects such as distributed loads over the beam have not been taken into account.

$$\begin{bmatrix} F_x \\ F_y \\ F_z \\ M_x \\ M_y \\ M_z \end{bmatrix} = \begin{pmatrix} \frac{24EI}{L^3} + \frac{2EA}{L} & 0 & 0 & 0 & 0 & 0 \\ 0 & \frac{24EI}{L^3} + \frac{2EA}{L} & 0 & 0 & 0 & 0 \\ 0 & 0 & \frac{48EI}{L^3} & 0 & 0 & 0 \\ 0 & 0 & 0 & \frac{8EI}{L} + \frac{2GJ}{L} & 0 & 0 \\ 0 & 0 & 0 & 0 & \frac{8EI}{L} + \frac{2GJ}{L} & 0 \\ 0 & 0 & 0 & 0 & 0 & \frac{16EI}{L} \end{pmatrix} \begin{bmatrix} u \\ v \\ w \\ \phi_x \\ \phi_y \\ \phi_z \end{bmatrix} \tag{4.4}$$

Unfortunately, the modulus of rigidity G of Ninjaflex was not provided in the manufacturers document, nor was it found in literature. For an isotropic material, there are multiple formulas that can be used to find the modulus of rigidity. This requires however, two of the following material constants:

- Young's modulus (E)
- Bulk modulus (K)
- Lame's first parameter (λ)
- Poisson's ratio (v)
- P-wave modulus (M)

The only listed and found parameter is the Young's modulus. This is why an estimation will be made for the modulus of rigidity from the table in Appendix C. For this report, Ninjatek will be considered as an incompressible material. Such a material has a poisson ratio of 0.5. From this,

the modulus of rigidity can be found.
The conversion formula for the modulus of rigidity can be found in the table C.1.

$$G = \frac{E}{2(1+\nu)} \tag{4.5}$$

This results in a modulus of rigidity of 4 MPa. Keeping in mind that this will not be exact due to the anisotropic nature of 3D-printing shown in the fabrication section 5.2. The table in Appendix C is only valid with homogeneous isotropic linear elastic materials. This means that the physical whisker could deviate from this.
The 6 DOF matrix in equation 7.1 will need to be reduced to 4 DOF matrix in the future. There is no interest in knowing the force in the z-direction or the moment around the z-direction as these degrees of freedom are not sought after for the whisker.

5 Fabrication

Unfortunately, due to COVID-19, it has been decided to keep this report purely theoretical. This part of the report will therefore only discuss the different materials used in the simulations and propose methods and advice on how to produce the suggested whisker.

5.1 Materials used

5.1.1 Ninjaflex

Ninjaflex TPU is a very flexible polyurethane material for FDM printers. It has a Young's modulus of 12 MPa. [19] This is just above the Young's modulus of rubber which is very low. A low young's modulus is useful because the beam will bend easily and thus bend the strain gauges more resulting in a larger difference in resistance. A decrease in the stiffness in the material will thus increase the responsivity of the sensor.

5.1.2 Carbon black doped TPU

The second material used to print the whisker is PI-ETPU 95-250 (ETPU). This TPU is doped with nanometric particles ranging between 50 nm to 100 nm have a very high melting temperature of 190° to 220°C [20]. This flexible material has a similar Young's modulus to Ninjaflex which is very useful because the material will bend similarly to the Ninjaflex TPU making the mechanical model and simulation model compatible with the carbon black doped TPU.

5.2 3D printing

The method of printing that was to be used is fusion deposition modelling (FDM). FDM is a method of additive manufacturing where layers of materials are fused together in a pattern to create an object. The material is melted past its glass transition temperature, and then extruded in a pattern next to or on top of previous extrusions, creating an object layer by layer [21].
There are a few advantages of FDM [22]:

- It is a very cost effective way to create custom parts.
- There is a wide range of thermoplastic materials available for prototyping and non-commercial applications.

There are also a few disadvantages coupled to FDM:

- FDM has a low dimensional accuracy and resolution compared to other methods.
- The end product will have visible layer lines
- The layered structure makes FDM parts inherently anisotropic

Especially the first disadvantage is important in this case. A low dimensional accuracy and resolution when using the printer to produce a thin beam will make every beam behave slightly differently. This could prove to have an impact on the properties of the beam.
An additional effect due to 3D printing is the so called warping 5.1. Warping is an effect that occurs during the cool down process of the structure. When the hot deposited layers are cooling down, they shrink. This causes the structure to tighten and slightly bend at the edges.

Figure 5.1: Warping of an FDM structure. [22]

Warping is an unwanted side effect of 3D-printing. It encourages non-linear effects and will therefore make the physical measurements more inaccurate. Methods to prevent warping [22] are:

- Avoid large flat areas
- Thin protruding features are prone to warping
- Sharp corners tend to warp more than round corners
- Different materials have a different susceptibility to warping.

For the whisker considered in this report, the whole structure consists of thin beams. There are also sharp corners and the strain gauges will consist of a different material. Three out of four causes for warping are present within the whisker. It is therefore fair to assume that warping will affect the physical whisker. The warping effect of thin beams could be counteracted by introducing extra sacrificial material at the edges of the beam in order to increase the surface area and therefore reducing the warping effect.

6 Results

The results will be shown by answering each of the research questions posed previously within the introduction section 1.2.1 of this report. The results primarily consist of comparisons between the mechanical analysis of the whisker basis and simulations of said whisker basis.

6.1 Answers to the research questions

6.1.1 Up until what loading of the whisker beam will the relations be linear?

The linear relations between applied forces and moments can be seen from the model section 4 of the report. Firstly, the 2 DOF linear relations for the applied load on the beam and the moment can be found in equation 3.20. The relation between the force in the x-direction and the deflection in the x-direction is described in equation 3.36.
For the 4 DOF linear relations, they are all described in equation 7.1.
In the previous sections of this report, there has not yet been a need to take non-linear effects into account. By choosing the beam dimensions in such a way that the beam is subject to Euler-Bernouilli beam theory, there are no non-linear effects to take into account. Additionally, the forces and moments have been chosen to be within the region which is still primarily provoking linear behaviour. This can be seen from the figures 6.5 to 6.9 which do not show any non-linear behaviour within the simulation results. In figure 6.1 can be seen that the ratio between the force and the displacement for the 2 DOF simulations is linear throughout the graph. This means that non-linear effects are not present in the simulations of the force. This cannot be said for figure 6.2 with the angle over the moment. In this figure, it can be seen that if a bigger force or moment would be applied to the beam, non-linear effects should be taken into account. The threshold for non-linearity is when a moment bigger than 0.04 N m is applied. This is similar for the 4 DOF simulations in figure 6.3 and 6.4. It can again be seen that the force to the x-direction is linear throughout the whole simulation and the moment to the angle. The fact that the force is linear throughout is not what is expected. What can be seen is that at a force of around 100 N, the displacement of the middle is about 23 mm. This is very unlikely to happen as the total distance from the middle to the edge of the beam is 25 mm.

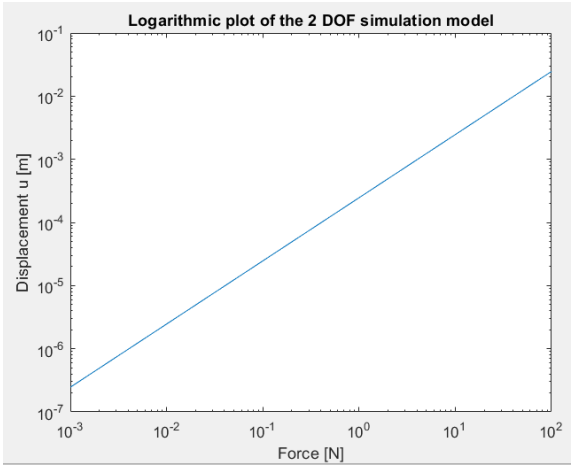

Figure 6.1: A logarithmic plot of the displacement of the 2 DOF beam with different forces in the x-direction. The straight line indicates that the simulation is linear.

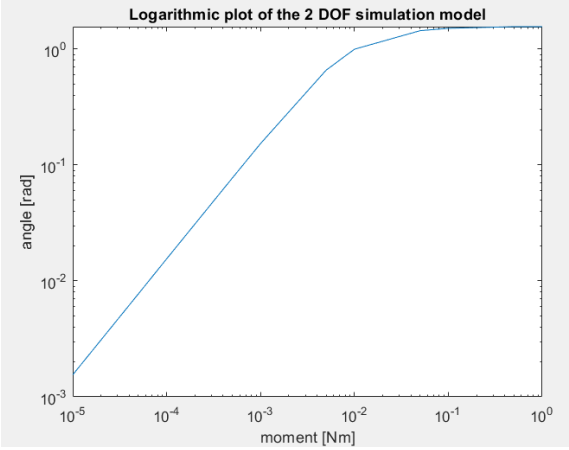

Figure 6.2: A logarithmic plot of the angle of the 2 DOF beam with different applied moments. Note the linearity until around 0.04 N m

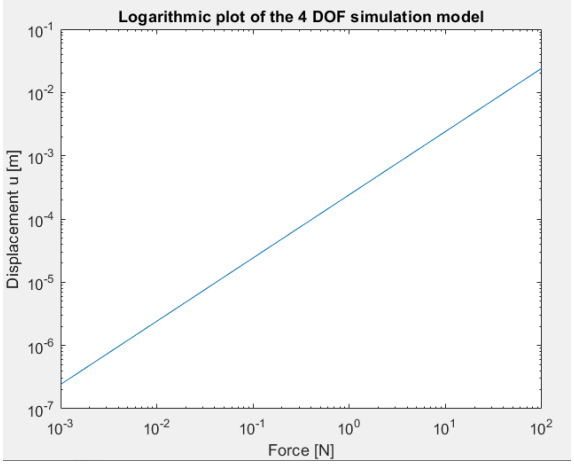

Figure 6.3: A logarithmic plot of the displacement of the 4 DOF cross beam with different forces in the x-direction. The straight line indicates that the simulation is linear.

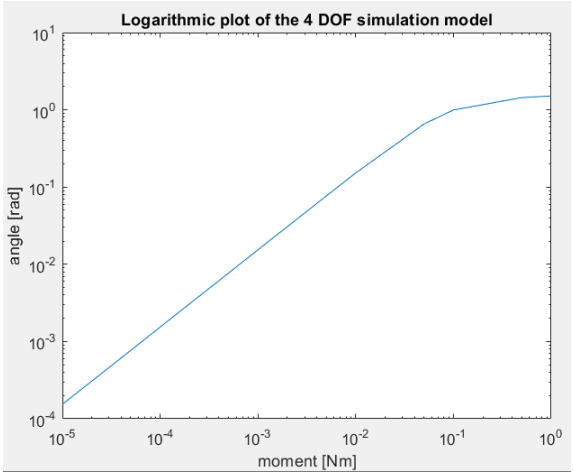

Figure 6.4: A logarithmic plot of the angle of the 4 DOF cross beam with different applied moments. Note the linearity until around 0.04 N m

6.1.2 To what degree are the relations between applied forces and moments on a whisker-inspired structure invertible?

The equations can be inverted by inverting the matrices in the equations. There is only one node on the 2 DOF and the 4 DOF beam that is loaded at a time. From equation 7.1 can be seen that the forces and the moments are each divided into 3 global coordinate components. The same is true for the deflection and the angle. This means that the element matrix will always be a 6 DOF square matrix. These matrices are invertible thus the relations will be as well. This does not take into account that loadings on the beam other than the whisker can be present. In that case, the 4 DOF equation would have to be changed to accomodate additional loads resulting in a non-square matrix. This would mean that the relations are not invertible. Within this report, the non-linear relations have not been considered. These relations are expected to be uninvertible.

6.1.3 What are the differences between the mechanical model and the simulations of a 3D-printed tactile whisker sensor in 2 DOF and 4DOF?

In order to compute and show the differences between the mechanical model and the simulations, the simulation data and the mechanical model have been analysed.
The results have been split into four parts. The comparison between the mechanical analysis and the simulations of the 2 DOF beam subject to a moment, the comparison between the mechanical analysis and the simulations of the 2 DOF beam subject to a force in the x-direction, the comparison between the mechanical analysis and the simulations of the 4 DOF beam subject to a moment and finally the comparison between the mechanical analysis and the simulations of the 4 DOF beam subject to a force in the x-direction. In order to validate the additivity of the directional components of the 4 DOF mechanical analysis, a force was simulated in the xy-direction and compared to the mechanical analysis. The same was done with a moment around the xy-axis.

2 DOF beam subject to a force

The first comparison done is between the forces acting in the x-direction of the beam. This was done by subjecting the 2 DOF beam to a force and then evaluate the deflection of the beam in the x-direction. The simulation as shown in Appendix A is expected to match up with equation 4.3. They are expected to have a linear relation between the force applied and the deflection in the x-direction. The comparison has been made in figure 6.5. What can be seen is that the mechanical analysis compares quite well to the simulation data. The simulation data seems linear and is deviating only 4 % from the mechanical analysis.

2 DOF beam subject to a moment

The second comparison is done by using the same piece of beam and subjecting it to a moment instead of a force. The Ansys simulation can be seen in Appendix A. The rotation of the middle of the beam is then compared between the simulation data and the mechanical analysis. As the analysis is linear and is within the limit of applied moment that is linear, it is expected that the simulation is linear.
From figure 6.6 it can be seen that the simulation data is indeed linear. The simulation data does resemble the mechanical analysis, however, there seems to be around a 10% difference between the two.

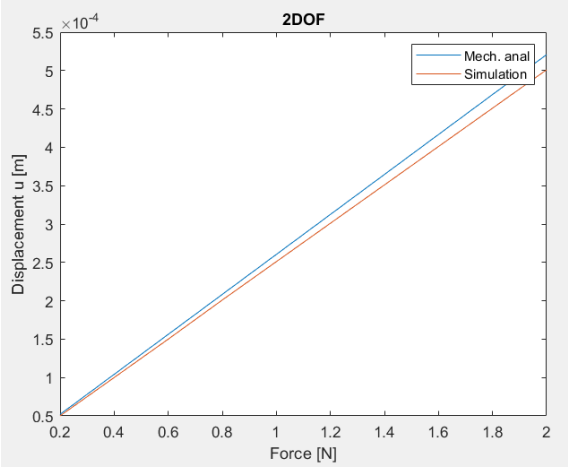

Figure 6.5: A comparison between the simulation data and the mechanical analysis of the 2 DOF beam subjected to a force in the x-direction.

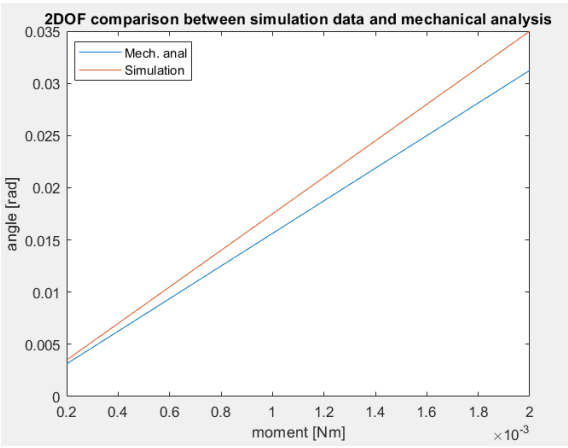

Figure 6.6: A comparison between the simulation data and the mechanical analysis of the 2 DOF beam subjected to a moment.

4 DOF beam subject to a force

The next step to take is to look at the differences and similarities between the force in the x-direction and the deflection for the 4 DOF cross beam. The Ansys simulation can be found in Appendix A. When looking at equation 7.1 it is expected that this relation will be linear as well. From figure 6.7 can be seen that this is indeed the case. The simulation data resembles the mechanical analysis very closely. The difference between the two is almost 0. The relation of force to displacement between the simulations and the mechanical analysis is even better in the 4 DOF case than for 2 DOF. This is not expected as the basis for the 4 DOF relations are the 2 DOF relations. It is therefore unlogical that the results are better for this case than the 2 DOF case.

4 DOF beam subject to a moment

In this section, the influence of the moment on the angle of the 4 DOF beam is analysed. The Ansys simulation can be found in Appendix A. Again, this relation is expected to be linear as can be seen from equation 7.1. When comparing the simulation data to the mechanical analysis in figure 6.8, it can be seen that both are linear. Again, the 4 DOF analysis and simulation

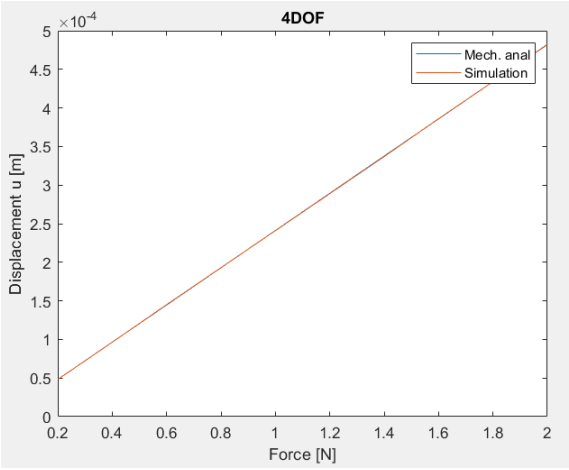

Figure 6.7: A comparison between the simulation data and the mechanical analysis of the 4 DOF beam subjected to a force in the x-direction.

data lie even closer together than they are for the 2 DOF whisker.

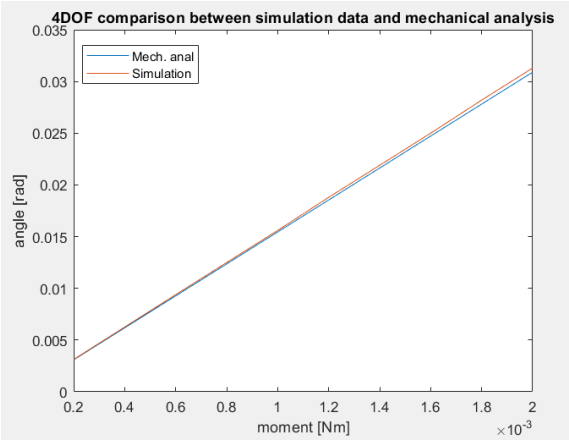

Figure 6.8: A comparison between the simulation data and the mechanical analysis of the 4 DOF beam subjected to a moment.

4 DOF beam subject to combined forces

After obtaining the results for the cases above, there is one important question to be answered. 'Can the components of the forces be combined?' This is important because so far, only a force in the x-direction has been considered. That is why a force in the xy-direction is applied to the 4 DOF cross beam. For simplicity, the x and the y components have been taken to be equal. From figure 6.9 can be seen that the simulation and the mechanical analysis lie close to each other. This means that the assumption that the each component of the forces can be added together in order to form the final direction of the force.

4 DOF beam subject to combined moments

It is also important to know that the moments in different directions can simply be added together. Figure 6.10 shows the response of the angle to the application of a moment around the x-axis and around the y-axis at the same time. It can be seen that the results are close together.

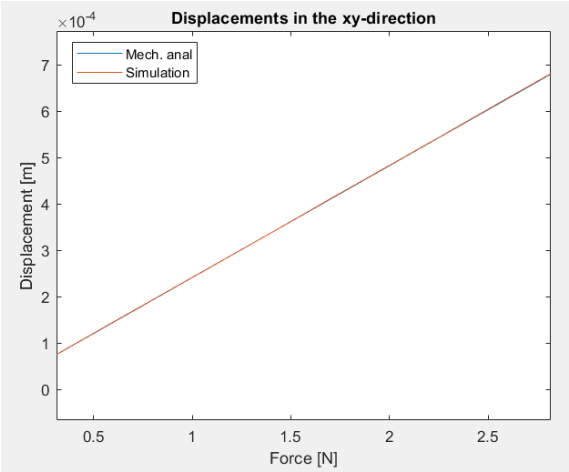

Figure 6.9: A comparison between the deflection of simulation data and the mechanical analysis of the 4 DOF beam subjected to a force in the xy-direction. In this figure, the total displacement can be seen on the y-axis and the total force applied can be seen on the x-axis.

They are not exactly the same as seen in figure 6.8. This could be due to some errors in the angle measurement of the simulations.

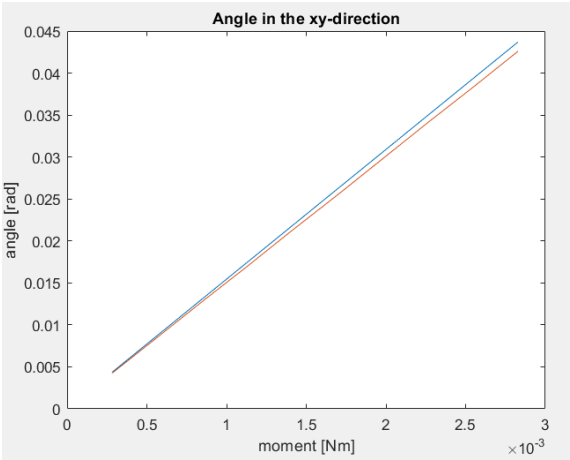

Figure 6.10: A comparison between the simulation data and the mechanical analysis of the 4 DOF beam subjected to a moment around the xy-axis.

6.2 Discussion

The model proposed within this report is mainly focused on the beams at the base of the whisker. This is where a mechanical analysis was made for the behaviour of the beams subjected to a force or a moment. Some of the results seem promising, others need more work. The mechanical relations of the forces and moments in the 4 DOF situation are very close to the simulations which is quite a promising result. The problem lies with the 2 DOF. Especially the moment to angle relation of the 2 DOF is quite peculiar and not what was expected. The simulation should not have a significantly bigger slope than the mechanical analysis. The error is about 10%. This can prove to be quite a lot when applying larger moments. There are a few reasons why this could be happening. The most obvious reason is that some of the material data is not correct in the Ansys simulation or an error could have been made with the simulation of the 2 DOF beam. As the 4 DOF mechanical model relies on the 2 DOF mechanical model and lies so close to the simulation data, it is unlikely that the mechanical analysis is wrong (this should of course not be completely ruled out). The simulation of the 2 DOF beam with a force in the x-direction seems close enough to the mechanical analysis to justify saying that it looks as if the mechanical analysis predicts the linear behaviour of the simulations well. The possibility exists for example that there is a small rounding error somewhere.
The physical whisker will however very likely not behave as described in the mechanical analysis. This is because the 3D-printed structure will be subject to multiple non-linear effects such as warping and anisotropic behaviour. Ninjaflex is also not likely to be a perfect incompressible material. This assumption was made for the mechanical model and Ninjaflex was taken to be a homogeneous isotropic linear elastic material in order to compute the modulus of rigidity. This is of course not the case for the physical whisker. More research will have to be done on this.

7 Conclusions and Recommendations

This section of the report will start by answering the main research question of this report within the conclusion. After this, recommendations will be given to future people aiming to improve on this assignment.

7.1 Conclusion

The main research question posed in the introduction was: 'What are the relations between applied forces and moments and the induced deformations on a whisker-inspired structure?' The short answer to this question is that the relations have partially been found. What was found are some promising linear relations for the 4 DOF cross beam. Equation 7.1 for the 4 DOF relations can be found below. For unknown reasons, the 2 DOF relations of the moment and force are still not exactly correct. Especially the simulations and the mechanical analysis of the 2 DOF whisker subjected to a moment are far apart with a 10% difference between each other. The non-linear relations have not been looked at because, within the scope of the forces and moments applied to the whisker in this report, the non-linear relations seem insignificant. The relations in the global coordinate system hold true as the results are positive when a force or moment is applied in a combination of directions. Equations 7.1 can simply be superimposed to get a correct end result.

$$\begin{bmatrix} F_x \\ F_y \\ F_z \\ M_x \\ M_y \\ M_z \end{bmatrix} = \begin{pmatrix} \frac{24EI}{L^3} + \frac{2EA}{L} & 0 & 0 & 0 & 0 & 0 \\ 0 & \frac{24EI}{L^3} + \frac{2EA}{L} & 0 & 0 & 0 & 0 \\ 0 & 0 & \frac{48EI}{L^3} & 0 & 0 & 0 \\ 0 & 0 & 0 & \frac{8EI}{L} + \frac{2GJ}{L} & 0 & 0 \\ 0 & 0 & 0 & 0 & \frac{8EI}{L} + \frac{2GJ}{L} & 0 \\ 0 & 0 & 0 & 0 & 0 & \frac{16EI}{L} \end{pmatrix} \begin{bmatrix} u \\ v \\ w \\ \phi_x \\ \phi_y \\ \phi_z \end{bmatrix} \tag{7.1}$$

7.2 Recommendations

7.2.1 Look at the effect of the ratio of the length over the thickness.

The first advice is to look closer into the ratio of the length over the thickness. Within the design section 2 of the report, an educated guess was made. This should be looked at and the optimal length over thickness should be found. This ratio will influence the linearity of the beam and the ratio of force that is converted into moment and force in the x-direction. This could also be investigated further. A suggestion would be to simulate the full whisker and put a force in the x-direction on the 2 DOF and 4 DOF whisker. Then, look how much of that force is converted into moment and force in the x-direction. Do this for different beam thicknesses, still trying to be within the linear range of the beam. This way, the effect of the length over the thickness can be derived.

7.2.2 Obtain more data about the material

For this report, it was assumed that the material is incompressible in order to make an estimation for the modulus of rigidity. It is advised to know the modulus of rigidity in the future to make a better mechanical model and simulation.

7.2.3 Look at non-linear effects

The range in which the forces and the moments were selected, was done in order to minimize non-linear effects, not to optimize the readings from the strain gauges. A bigger force is likely

to give a more distinguished reading on the strain gauges but will also encourage non-linear effects. Being able to model this correctly, would in turn make more distinguished readings possible and therefore improve the overall whisker.
As the beams are suspended in a fixed-fixed fashion, deformation will introduce axial loading in the beams. This will result in beam stiffening and nonlinear responses. One may try to incorporate this in the same Galerkin based method. The starting equation would be:

$$EI\frac{d^4u}{dy^4} + P\frac{d^2u}{dy^2} = q(y) \tag{7.2}$$

7.2.4 Research into the whisker itself

Within this report, the focus lies on creating a mechanical analysis of the behaviour of the whisker. However, during this research, only the beam at the base of the whisker was analysed and not the whisker beam itself. Although this was not done, it should theoretically be possible to compute the ratio between the force on the whisker and height at which this is applied by using beam element equation 3.20.

7.2.5 Strain-gauges

Further research can be done into adding additional strain-gauges in order to measure the full 6 DOF. A possible addition could be adding torsional sensors into the beams. These sensors would be able to distinguish between pushing the whisker in the x- or y-direction and pushing the whisker down or twisting it. This allows a force in the z-direction on the whisker and a moment around the z-axis on the whisker to be recognised as such due to them being the only 2 movements of the whisker that do not cause a twist to occur in the beams at the base of the whisker.

A Appendix 1: Simulation models for the 2 DOF and 4 DOF beams

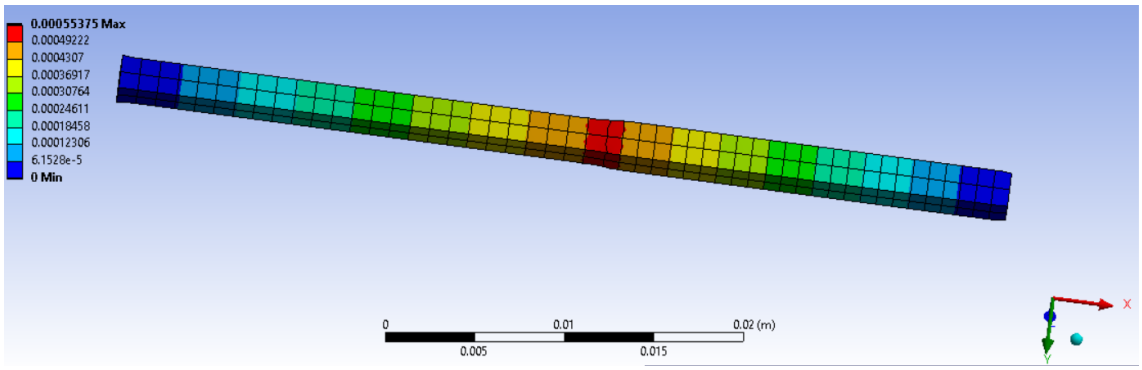

Figure A.1: Result of the deflection of the Ansys simulation when a force in the x-direction is applied to the 2 DOF beam. The red color corresponds to the section with the biggest deflection and the blue color to the smallest amount of deflection in m.

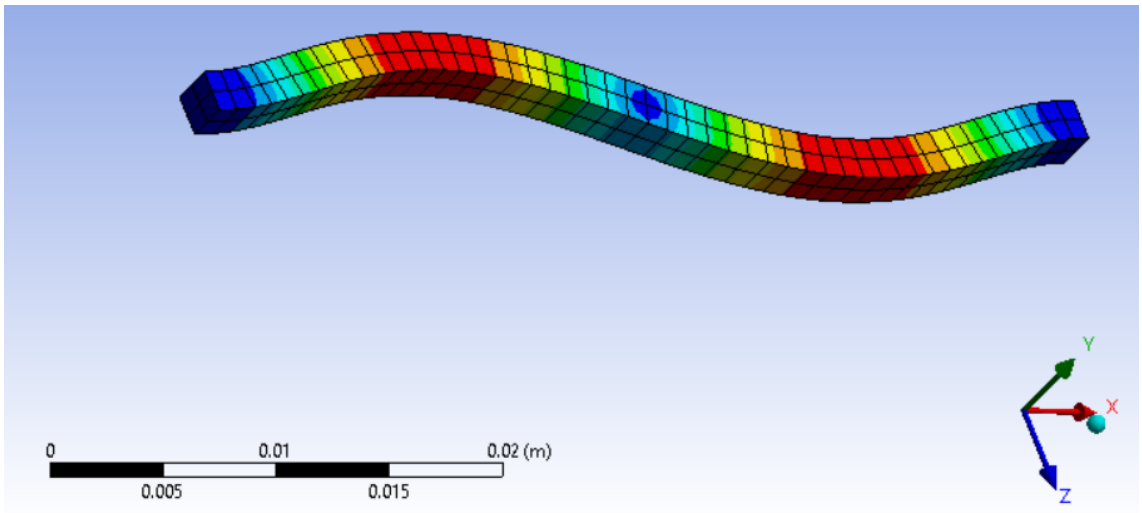

Figure A.2: Result of the deflection of the Ansys simulation when a moment around the y-axis is applied to the 2 DOF beam. The red color corresponds to the section with the biggest deflection and the blue color to the smallest amount of deflection in m.

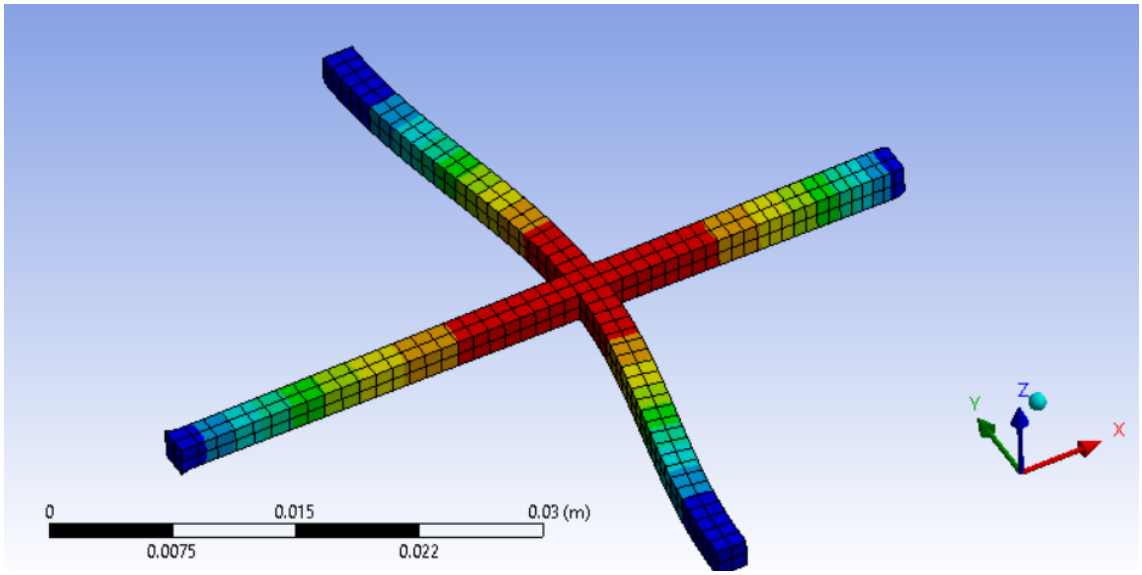

Figure A.3: Result of the deflection of the Ansys simulation when a force in the x-direction is applied to the 4 DOF beam. The red color corresponds to the section with the biggest deflection and the blue color to the smallest amount of deflection in m.

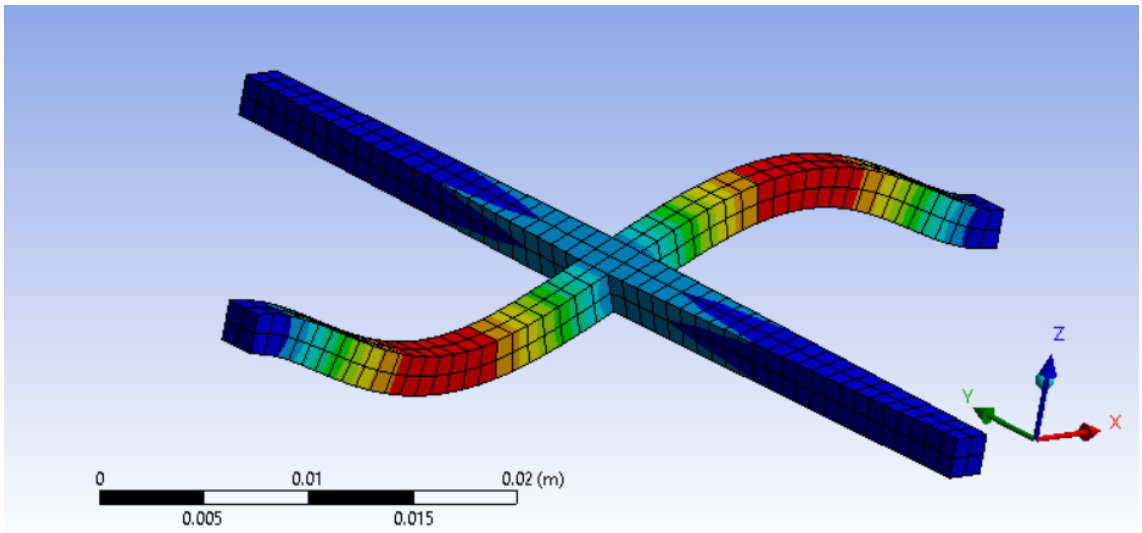

Figure A.4: Result of the deflection of the Ansys simulation when a moment around the y-axis is applied to the 4 DOF beam. The red color corresponds to the section with the biggest deflection and the blue color to the smallest amount of deflection in m.

B Appendix 2: full matrix for a beam element in global coordinates

$$\begin{bmatrix} F_{1x} \\ F_{1y} \\ F_{1z} \\ M_{1x} \\ M_{1y} \\ M_{1z} \\ F_{2x} \\ F_{2y} \\ F_{2z} \\ M_{2x} \\ M_{2y} \\ M_{2z} \end{bmatrix} = \begin{bmatrix} \frac{EA}{L} & 0 & 0 & 0 & 0 & 0 & -\frac{EA}{L} & 0 & 0 & 0 & 0 & 0 \\ 0 & \frac{12EI}{L^3} & 0 & 0 & 0 & \frac{6EI}{L^2} & 0 & -\frac{12EI}{L^3} & 0 & 0 & 0 & \frac{6EI}{L^2} \\ 0 & 0 & \frac{12EI}{L^3} & 0 & -\frac{6EI}{L^2} & 0 & 0 & 0 & -\frac{12EI}{L^3} & 0 & -\frac{6EI}{L^2} & 0 \\ 0 & 0 & 0 & \frac{GJ}{L} & 0 & 0 & 0 & 0 & 0 & -\frac{GJ}{L} & 0 & 0 \\ 0 & 0 & -\frac{6EI}{L^2} & 0 & \frac{4EI}{L} & 0 & 0 & 0 & \frac{6EI}{L} & 0 & \frac{2EI}{L} & 0 \\ 0 & \frac{6EI}{L^2} & 0 & 0 & 0 & \frac{4EI}{L} & 0 & -\frac{6EI}{L^2} & 0 & 0 & 0 & \frac{2EI}{L} \\ -\frac{EA}{L} & 0 & 0 & 0 & 0 & 0 & \frac{EA}{L} & 0 & 0 & 0 & 0 & 0 \\ 0 & -\frac{12EI}{L^3} & 0 & 0 & 0 & -\frac{6EI}{L^2} & 0 & \frac{12EI}{L^3} & 0 & 0 & 0 & -\frac{6EI}{L^2} \\ 0 & 0 & -\frac{12EI}{L^3} & 0 & \frac{6EI}{L^2} & 0 & 0 & 0 & \frac{12EI}{L^3} & 0 & \frac{6EI}{L^2} & 0 \\ 0 & 0 & 0 & -\frac{GJ}{L} & 0 & 0 & 0 & 0 & 0 & \frac{GJ}{L} & 0 & 0 \\ 0 & 0 & -\frac{6EI}{L^2} & 0 & \frac{2EI}{L} & 0 & 0 & 0 & \frac{6EI}{L} & 0 & \frac{4EI}{L} & 0 \\ 0 & \frac{6EI}{L^2} & 0 & 0 & 0 & \frac{2EI}{L} & 0 & -\frac{6EI}{L^2} & 0 & 0 & 0 & \frac{4EI}{L} \end{bmatrix} \begin{bmatrix} u_1 \\ v_1 \\ w_1 \\ \phi_{1x} \\ \phi_{1y} \\ \phi_{1z} \\ u_2 \\ v_2 \\ w_2 \\ \phi_{2x} \\ \phi_{2y} \\ \phi_{2z} \end{bmatrix} \tag{B.1}$$

C Appendix 3: table with all the relations between material constants

	$K =$	$E =$	$\lambda =$	$G =$	$\nu =$	$M =$	Notes
$(K,\ E)$			$\frac{3K(3K-E)}{9K-E}$	$\frac{3KE}{9K-E}$	$\frac{3K-E}{6K}$	$\frac{3K(3K+E)}{9K-E}$	
$(K,\ \lambda)$		$\frac{9K(K-\lambda)}{3K-\lambda}$		$\frac{3(K-\lambda)}{2}$	$\frac{\lambda}{3K-\lambda}$	$3K-2\lambda$	
$(K,\ G)$		$\frac{9KG}{3K+G}$	$K-\frac{2G}{3}$		$\frac{3K-2G}{2(3K+G)}$	$K+\frac{4G}{3}$	
$(K,\ \nu)$		$3K(1-2\nu)$	$\frac{3K\nu}{1+\nu}$	$\frac{3K(1-2\nu)}{2(1+\nu)}$		$\frac{3K(1-\nu)}{1+\nu}$	
$(K,\ M)$		$\frac{9K(M-K)}{3K+M}$	$\frac{3K-M}{2}$	$\frac{3(M-K)}{4}$	$\frac{3K-M}{3K+M}$		
$(E,\ \lambda)$	$\frac{E+3\lambda+R}{6}$			$\frac{E-3\lambda+R}{4}$	$\frac{2\lambda}{E+\lambda+R}$	$\frac{E-\lambda+R}{2}$	$R=\sqrt{E^2+9\lambda^2+2E\lambda}$
$(E,\ G)$	$\frac{EG}{3(3G-E)}$		$\frac{G(E-2G)}{3G-E}$		$\frac{E}{2G}-1$	$\frac{G(4G-E)}{3G-E}$	
$(E,\ \nu)$	$\frac{E}{3(1-2\nu)}$		$\frac{E\nu}{(1+\nu)(1-2\nu)}$	$\frac{E}{2(1+\nu)}$		$\frac{E(1-\nu)}{(1+\nu)(1-2\nu)}$	
$(E,\ M)$	$\frac{3M-E+S}{6}$		$\frac{M-E+S}{4}$	$\frac{3M+E-S}{8}$	$\frac{E-M+S}{4M}$		$S=\pm\sqrt{E^2+9M^2-10EM}$ There are two valid solutions. The plus sign leads to $\nu \geq 0$. The minus sign leads to $\nu \leq 0$.
$(\lambda,\ G)$	$\lambda+\frac{2G}{3}$	$\frac{G(3\lambda+2G)}{\lambda+G}$			$\frac{\lambda}{2(\lambda+G)}$	$\lambda+2G$	
$(\lambda,\ \nu)$	$\frac{\lambda(1+\nu)}{3\nu}$	$\frac{\lambda(1+\nu)(1-2\nu)}{\nu}$		$\frac{\lambda(1-2\nu)}{2\nu}$		$\frac{\lambda(1-\nu)}{\nu}$	Cannot be used when $\nu=0 \Leftrightarrow \lambda=0$
$(\lambda,\ M)$	$\frac{M+2\lambda}{3}$	$\frac{(M-\lambda)(M+2\lambda)}{M+\lambda}$		$\frac{M-\lambda}{2}$	$\frac{\lambda}{M+\lambda}$		
$(G,\ \nu)$	$\frac{2G(1+\nu)}{3(1-2\nu)}$	$2G(1+\nu)$	$\frac{2G\nu}{1-2\nu}$			$\frac{2G(1-\nu)}{1-2\nu}$	
$(G,\ M)$	$M-\frac{4G}{3}$	$\frac{G(3M-4G)}{M-G}$	$M-2G$		$\frac{M-2G}{2M-2G}$		
$(\nu,\ M)$	$\frac{M(1+\nu)}{3(1-\nu)}$	$\frac{M(1+\nu)(1-2\nu)}{1-\nu}$	$\frac{M\nu}{1-\nu}$	$\frac{M(1-2\nu)}{2(1-\nu)}$			

Figure C.1: Table showing the relations between different material constants. [23]

Bibliography

[1] T. Prigg, D. Goldreich, G. E. Carvell, and D. J. Simons, "Texture discrimination and unit recordings in the rat whisker/barrel system," *Physiology & Behavior*, vol. 77, no. 4, pp. 671 – 675, 2002.

[2] A. S. Ahl, "The role of vibrissae in behavior: A status review," *Veterinary Research Communications*, vol. 10, pp. 245–268, 1986.

[3] W. Hanke, M. Witte, L. Miersch, M. Brede, J. Oeffner, M. Michael, F. Hanke, A. Leder, and G. Dehnhardt, "Harbor seal vibrissa morphology suppresses vortex-induced vibrations," *Journal of Experimental Biology*, vol. 213, no. 15, pp. 2665–2672, 2010.

[4] O. Bebek and M. C. Cavusoglu, "Whisker sensor design for three dimensional position measurement in robotic assisted beating heart surgery," in *Proceedings 2007 IEEE International Conference on Robotics and Automation*, pp. 225–231, 2007.

[5] J.Tichelaar, "3d-printed implementation of a tactile pressure sensor working in multiple dof," 2018.

[6] B. Eijking, R. Sanders, and G. Krijnen, "Development of whisker inspired 3d multi-material printed flexible tactile sensors," in *2017 IEEE SENSORS*, pp. 1–3, 2017.

[7] S. Harada, W. Honda, T. Arie, S. Akita, and K. Takei, "Fully printed, highly sensitive multifunctional artificial electronic whisker arrays integrated with strain and temperature sensors," *ACS Nano*, vol. 8, no. 4, pp. 3921–3927, 2014. PMID: 24580035.

[8] R. P. M. Lungarella, V. V. Hafner and H. Yokoi, "An artificial whisker sensor for robotics," *IEEE/RSJ*, vol. 3, pp. 2931–2936.

[9] M. Kaneko and T. Tsuji, "A whisker tracing sensor for manufacturing application," *IFAC Proceedings Volumes*, vol. 33, no. 26, pp. 383 – 388, 2000. IFAC Conference on Mechatronic Systems, Darmstadt, Germany, 18-20 September 2000.

[10] D. F. Cirak, "Finite element formulation for beams."

[11] Bbanerje, "Deformation of a timoshenko beam (blue) compared with that of an euler-bernoulli beam (red)."

[12] C. Du Toit, "The continuous galerkin finite element method as applied to the 1d beam equation: A systems approach," pp. 331–338, 01 2006.

[13] D. L. Logan, *First Course in the Finite Element Method*. 2007.

[14] M. Tawfik, *Finite Element Analysis (Book Draft)*. 01 2020.

[15] H. B. Young W. Kwon, *Finite element method using MATLAB*. 2018.

[16] K. Grammol, "Uniaxial deflection - constant load, area and stiffness."

[17] P. GODBOLE, R. SONPAROTE, and S. DHOTE, *MATRIX METHODS OF STRUCTURAL ANALYSIS*. PHI Learning, 2014.

[18] J. Carrer, W. Mansur, R. Scuciato, and S. Fleischfresser, "Analysis of euler-bernoulli and timoshenko beams by the boundary element method," pp. 2333–2349, 07 2012.

[19] F. Inc., “Ninjatek technical specifications.”

[20] E. P. Lorea, “3d printed sensor to detect muscle contraction by means of force myography,” November 2017.

[21] E. Grames, “Fdm (3d printing) - simply explained,” 2019.

[22] A. B. Varotsis, “Introduction to fdm 3d printing.”

[23] wikipedia, “Shear modulus.”